Analyses of eddies in the Skagerrak

A study based on NorKyst800 model results

Birger O. Vogt

Thesis submitted for the degree of
Master in Geosciences: Meteorology and Oceanography
60 credits

Department of Geosciences
Faculty of mathematics and natural sciences

UNIVERSITY OF OSLO

Spring 2016

Analyses of eddies in the Skagerrak

A study based on NorKyst800 model results

Birger O. Vogt

Analyses of eddies in the Skagerrak

http://www.duo.uio.no/

Printed: Reprosentralen, University of Oslo

Abstract

It is well known that cyclonic and anticyclonic eddies are numerous in the Skagerrak. Nevertheless a systematic analysis of their statistics appears to be missing. This is the topic of the present thesis in which we investigate the frequency of their appearance, whether they have preferred areas of occurrence, the number of cyclones versus anticyclones, and their sizes. In addition we perform a kinetic energy analysis in which we discriminate between the kinetic energy associated with the mean motion (the mean kinetic energy, MKE) and the energy associated with the variance (the eddy kinetic energy, EKE). The rationale is to investigate whether there is a correlation between the EKE and the preferred areas of occurrence, if any. The "data" we use are the 24 hour average daily snapshots produced by MET Norway's operational coastal ocean forecasting model NorKyst800. The period we study is the two years 2013 and 2014 which results in about 700 snapshots. The eddy detection method we use is the so called Okubo-Weiss method. We find that overall there are more cyclones than anticyclones, that there is a strong correlation between kinetic energy and generation of eddies, that in general that most of the eddies prefer to be within the Norwegian Trench area, and that the eddies are more frequent in three specific areas along the Trench, namely the inner and deepest part of the Trench, outside of Torungen/Arendal and south Lista at the the southern tip of Norway.

Acknowledgements

I would like to extend my greatest appreciation and sincere thanks to my family for being very supportive of me, Martha Trodahl for technical support with debugging. And last but definitely not least my supervisor Lars Petter Røed

Blindern June 15, 2016
Birger Vogt (sign.)

Contents

List of Figures

Chapter 1

Introduction

It is well known that eddies are numerous in the Skagerrak (e.g., *Røed and Fossum*, 2004; *Fossum*, 2006; *Albretsen and Røed*, 2006; *Røed and Albretsen*, 2007; *Albretsen*, 2007; *Albretsen and Røed*, 2010, and references therein). Nevertheless it appears that no one has studied the eddy statistics, which is the topic of this thesis.

1.1 Circulation in the Skagerrak basin

The most conspicous topographic feature in the Skagerrak is the Norwegian Trench, which cuts into the Skagerrak following the Norwegian coast (Figure 1.1). While its mean depth is about 210m, its maximum depth is 710m deep in its inner part in the middle of Skagerrak. The bottom slope in a barotropic fluid acts like a β effect, but instead of limiting north-south motion, topography inhibits motions across the depth contours, also referred to as the topographic β effect. So random movement over a slope should give an inverse cascade and generate jets along the topographic slope (*Vallis and Maltrud*, 1993).

There are three main sources of water masses that flows into the Skagerrak basin. An inflow of warm and salt Atlantic water that follows the southern slope of the Norwegian trench, south of the Trench, along the shallow coast of Denmark we have the Jutland current from the southern North Sea and the German Bight, carrying relativly cold and fresh water. Finally, up along the west coast of Sweden, through Kattegat comes a current of brackish water from the Baltic Sea.

Outside the tip of Skagen all these three currents meets, and we see a host of mesoscale eddies in the front between these two currents while they mix and move northwards up along the Swedish coast just south of Koster (Figure 1.2). Here it turns westwards and follows the Norwegian coast as the Norwegian Coastal Current (NCC). As it runs along the coast it mixes with freshwater from river runoffs (*Sætre*, 2007). It leaves the Skagerrak proper just south of Norway's southern tip, that is, at Lista where, according to *Røed and Fossum* (2004), an anticyclonic eddy frequently appears. Thus the pattern of the general circulation in Skagerrak is that of a cyclonic gyre (Figure 1.1). As we see from this figure the currents are not entirely separated and the Jutland current and the Atlantic water intrusion can also mix west of Denmark while entering the Skagerrak basin.

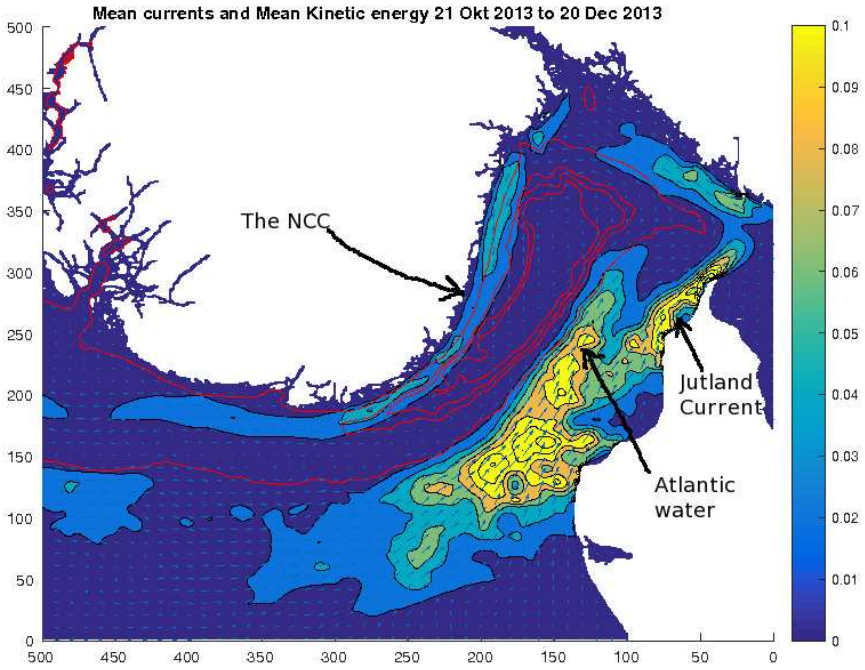

Figure 1.1: The illustration is from a 'typical' 60 day mean of the currents in Skagerrak. The colorbar indicates the mean kinetic energy (m^2/s^2) which is a measure of the strenght of the current. The arrows gives the current direction. The red lines shows the ocean depth contours for 200m, 400m, 450m and 500m depth and outlines the Norwegian trench.

1.2 Instability mechanisms in the Skagerrak

According to *Fossum and Røed* (2006) and *Fossum* (2006) eddies in the Skagerrak form due to barotropic as well as baroclinic instabilities. Barotropic instability is an instability that arises because of the horizontal shear in a flow, and may occur in fluids of constant density. It is important for two reasons. First it is important in its own right as an instability mechanism for jets and vortices, and as an important for geostrophic turbulence. Second, many problems in barotropic and baroclinic instability are formally and dynamically similiar, so that the solutions and insight we obtain in the often simpler problems in barotropic instability may be useful in the baroclinic problem (*Vallis*, 2006). To determine whether a current is likely or not to become bartropically unstable, its usually analysed with the Rayleigh-Kyo or Fjørtoft criteria, both of which gives neccessary but not sufficient conditions for instabilities to occur. Although there are very few, if any, cases where instabilities do not occur if the current satisfies the Fjørtoft criterion.

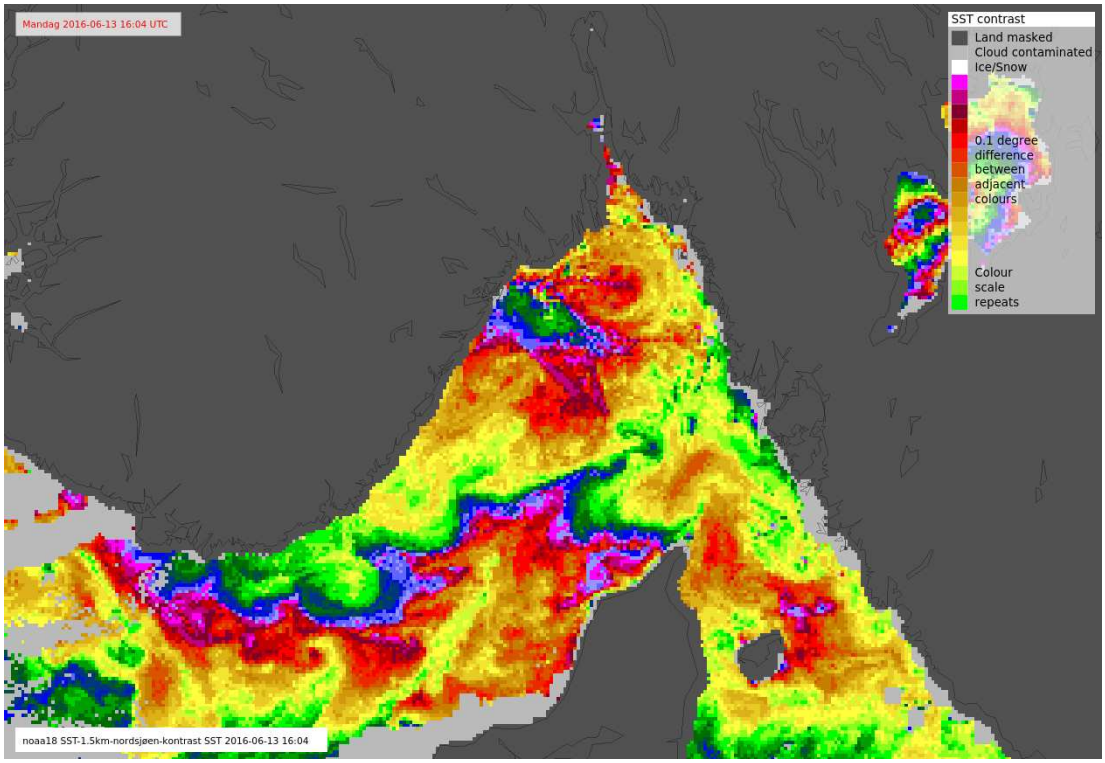

Figure 1.2: Displayed is a satellite imagery of the sea surface temperature (SST) contrast on June 13, 2016 at 16UTC (Courtesy of OSI-SAF). The color bar indicates temperature differences of 0.1 degree C and is a wrap around. Note the many mesoscale features present which is typical for these kind of images.

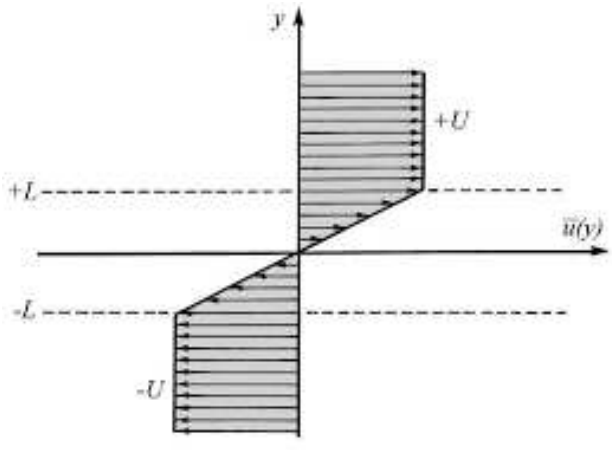

Figure 1.3: This is an idealised example of the Kelvin Helmholtz model of barotropic instability in the horizontal direction.Taken from Benoit Cushman-Roisin's upcoming book,Environmental Fluid Mechanics. (*Cushman-Roisin*, 2016)

1.2.1 Barotropic instability mechanisms

Regarding barotric instabilities, the β effect helps to stabilise easterly moving jets and can contribute to destabilising westwards moving ones. Therefore its more more likely that we will see instabilities in the NCC along the southeastern Norwegian coast between the inflowing and outflowing jets (Figure 1.1) than in the inflowing Atlantic water along the Danish coast. In addition we do not expect to see eddies inside the jets. The rationale is that as an eddy comes into contact with strong jets, they are more likely to be pulled apart or be wiped out. Rather we would from barotropic instability theory expect to see them at the edges or outside of the jets.

One of the mechanism for barotropic instability is the Kelvin-Helmholtz instability. The idea is that two edge-waves generated by two jets of different strenghts or orientation that run parallell to each other separated by a relative calm region, as exemplified in Figure 1.3, can feed back on each other and couple to form a single growing mode (*Vallis*, 2006). This occurs particularly for long wavelenghts, as the cross stream decay scale of an edge wave is proportional to its along stream wavelenght. If this is the case and if the edge waves have the appropriate phase with respect to each other, this will result in an instability. This instability mechanism also predicts that the perturbation will tilt into the shear and develop as shown by *Vallis* (2006) (his Fig. 1.3 on page 256).

In our case the jets are the NCC and the North Atlantic intrusion along the southern slope of the Trench. However its hard to judge without going deeply into mathematics whether this model would be applicable in our case. It may be that the area between the two jets is too broad for the edge waves to penetrate, but as the lenght of the jets are much longer than the distance between them, it is indeed possible. Thus it may look like barotropic instability might be important for our domain. However a proper instability analysis would be required to know for certain.

1.2.2 Baroclinic instability

Baroclinic instabilities arise from perturbations in fluids with a horizontal density gradients. These density gradients means that a horizontal mixing results in the centre of gravity decreasing giving a lowering of the potential energy, which will then be freed and give a gain in kinetic energy to the perturbation mixing them. Thus the perturbation will be amplified and grow, which will lead to an instability. These processes are one of the reasons why eddies are very important for both stirring and mixing in the ocean and why we are so interested in them.

1.3 Previous studies

Petersen et al. (2013) performed a seven year simulation with a global high resolution z-coordinate model (the POP model) utilizing the Boussinesq approximation. Their grid varies from 11 km grid resolution at the equator to 3 km at the poles. They characterised eddies using the R^2 method and took a systematic eddy census of a three dimensional global ocean simulation to provide statistical information throughout the global ocean. In this they removed eddies lasting less than four weeks. Hence the eddies we are looking at in our study are considered as noise in their

study.

Røed and Fossum (2004) looked into mean and eddy motion in the Skagerrak/northern North Sea analysing results from a two year simulation with a terrain-following, σ-coordinate ocean model (the MIPOM model). The grid resolution was 4km. They found that much of the variability was caused by reccurent anticyclonic eddies in the Lista area, and considered possible mechanisms whereby cyclogenisis could occur in the area.

Albretsen and Røed (2010) investigated the resolution neccessary to accurately represent mesoscale climatology in the Skagerrak northern/North Sea. To this end they performed four 27 year long simulations with two different terrain-following models, namely the MIPOM model (*Blumberg and Mellor*, 1987) and the ROMS model (*Haidvogel et al.*, 2008). In this, they applied two different grid resolutions, namely 4 km and 1.5 km respectively. The rationale was to explore whether the ROMS model proved more accurate than the older MIPOM model. They found that in the Skagerrak area, a fully, eddy resolving model is required to accurately capture the mesoscale activity in the region. The 4 km proved too coarse, and they assumed that a model with a grid resolution of 1 - 2 km or better would be required. In the ROMS 1.5 km model they found that the eddy kinetic energy was intensified over the depths of the Norwegian Trench, which was not apparent in the 4 km model versions. They assumed this was due to eddies too small to be resolved by the 4 km models.

Chelton et al. (2007) utilised an automated eddy-tracking procedure based on the Okubo-Weiss parameter and the methods outlined in *Isern-Fontanet et al.* (2003, 2006). They examined ten years of SSH fields constructed from altimetry data, tracking large scale eddies with diameters between 100-200 km over the world oceans. They found that these could account for much of the variability. While the scale is entirely unapplicable for our domain, the detection scheme is similar to the detection method used below (Section 2).

1.4 Present study

We analyse 24 hour average daily snapshots from the NorKyst800 model (*Albretsen et al.*, 2011). Results from this model are available since June 27, 2012, but we restrict the period to the two years 2013 and 2014. NorKyst800 runs operationally at the Norwegian Meteorological Institute (MET Norway), and is a version of the Regional Ocean Modeling System - ROMS (*Haidvogel et al.*, 2008; *Shchepetkin and McWilliams*, 2009).

As the name indicates the NorKyst800 model has a grid size of approximately 800 m. A common measure of the model's ability to support eddies is the number of grid cells per internal Rossby radius of deformation, say $N_r = L_r/\Delta s$ where L_r is the Rossby radius of deformation and Δs is the grid size. The rule of thumb is that $N_r \geq 10$ is required to be able to properly resolve L_r and to support generation of instabilities (*Røed*, 1996). As our domain has a Rossby radius between 10-16 km, a model with a grid size between 1 and 1.5 km is necessary to be fully eddy resolving. Our model's grid size is 800 m which gives $N_r \sim 12 - 20$, and thus satisfies this criterion.

We utilize these model results to make an eddy census of eddies in the Skagerrak. The advantage of using model results compared to, e.g., altimetry data (*Johannessen et al.*, 1989) is that

the model provides a near continuous series of images, while satellite imagery has large gaps due to cloud cover. In particular this is true for the Skagerrak area. Moreover, and equally important, is that the NorKyst800 model's grid size provides higher resolution images. As such this is the first attempt to make an eddy census of mesoscale structures and eddies in the Skagerrak based on a fully, eddy resolving model.

Chapter 2

Methods

To get insight into where anticyclones and cyclones are most frequent in Skagerrak we have analyzed results from the model NorKyst800 for the two years 2013 and 2014. The analysis is based on model results and model result only. No data have been used to verify or validate the results of the analysis.

2.1 The NorKyst800 model

NorKyst800 (*Albretsen et al.*, 2011) is a numerical, high-resolution, ocean modelling system, and is based on the Regional Ocean Modeling System - ROMS (*Haidvogel et al.*, 2008; *Shchepetkin and McWilliams*, 2009). It was originally initiated and developed as a cooperation between the Institute for Marine Research (IMR), the Norwegian Meteorological Institute (MET Norway) and the Norwegian Institute for Water Research (NIVA). We utilise the results from the NorKyst800 version running operationally at MET Norway. This version was created to provide environmental information for all coastal areas in Norway to serve as an aid in emergency services such as drift of oil and floating objects ('man-over-board'), spread of harmful algae and salmon lice, and the transport as well as dispersion of contaminants. It is also used as an intermediate model transferring information from the coarse 4 km deep ocean models to even finer scale fjord models with 150-200 m horizontal resolution (*Røed et al.*, 2016).

NorKyst800 has a grid of 2600x900 cells where each spans an area of 800mx800m. It utilizes a modified terrain-following s-coordinates in the vertical. It uses bathymetry data implemented from Statens Kartverk's Norge Digitalt database (norgedigitalt.no). The version we use has an open boundary where results from a coarser 4 km version of ROMS is used as input. The necessary atmospheric input is extracted from the AROME-MetCoOp model that runs operationally at MET Norway (*Müller et al.*, 2015). It utilises a modified Arakawa C-grid to stagger the variables, with density and sea surface height (and thus also pressure) calculated at the centre of the cells with velocity staggered to the edges of the cell.

As alluded to in Section 1.4 the grid size improvement compared to previous models with a 4 km horizontal resolution is essential to be able to capture mesoscale structures and eddies in Skagerrak. As shown below in Section 3.1 (cf. Figure 3.1 on page 12) it is evident that portion

of them have a radius of 4 km or less, which are unresolved by models of 4 km grid size.

2.2 Eddy detection method

To detect cyclones and anticyclones and make an eddy census we have used the Matlab toolbox by Pierrick Penven (*Penven et al.*, 2005) included in the ROMSTOOLS package freely available at http://www.simocean.org.za/tooleddy.php. This package employs the Okubu-Weiss Algorithm coupled with sea surface height (SSH) anomalies to avoid well known problems in the Okubo-Weiss method as outlined by *Basdevant and Philipovitch* (1994). The package was made to accept input of altimetric data with a resolution of about 30 km using longitude and latitude as coordinates. To accept input from the NorKyst800 xy-coordinate system we had to develop a program to translate form NorKyst800m corrdinates to latitude-longitude coordinates which is not trivial in itself. In addition the Matlab toolbox had to be changed to allow the NorKyst800 high resolution data to be utilised.

2.2.1 The Okubo-Weiss algorithm

The Okubo Weiss Algorithm is a tried and tested method for finding eddies in two dimensional flow fields. It is based on the theory of singularities, or critical point theory, and the findings of *Okubo* (1970). It analytically explored and identified different types of singularities in the flow field. These are points where the velocity components vanish simultaneously and where streamlines can meet, and thus are stationary points of flow. In this paper it is concluded that a necessary condition for vorticies to form is that

$$\lambda_{1,2} = \frac{1}{2}\left(\gamma + \sqrt{\alpha^2 \pm h^2 - \eta^2}\right) \tag{2.1}$$

have to be complex conjugates or purely imaginary. This is achieved if

$$\eta^2 \geq \alpha^2 + h^2. \tag{2.2}$$

Here γ is the divergence, η is the vorticity, α is the stretching deformation, and h is the shearing deformation. Thus (2.2) says that the vorticity must be larger than or equal to the deformation for a spiral to be a spiral. As concluded by *Okubo* (1970) if the divergence γ is negative then the trajectories are spirals that wind around and approach the origin as its limit. In this case the origin is a stable spiral point and when rotation is added this entails that we have a cyclone. If the divergence γ is positive then the trajectories are spirals that unwind and the trajectories move away from the origin without limit. In this case the origin is an unstable spiral point, and when rotation is added this entails that we have an anticyclone. If there is no divergence then both λ_1 and λ_2 are purely imaginary. In this case the trajectories form ellipses with centers at the origin in which case the motion is a stable one about the origin, which may be called a vortex point.

To find the center of the eddies we have to find spots where the geostrophic velocities are both zero, that is, points that *Okubo* (1970) refers to as "spiral point" or vortex points. To hit

such spots in a finite difference grid is quite unlikely. Instead we are forced to look for grid points where the absolute value of the velocity is minimum. Furthermore we have to assume that these points are sufficiently close to the points where the velocity components actually vanish simultaneously. The latter is a reasonable assumption and something we actually can achieve and test for with our 800 m grid model.

This result is quite similar to what *Weiss* (1991) found, coming at it from a different angle while exploring the dynamics of enstrophy transfers. As a result he came up with what is later referred to as the Okubo-Weiss parameter (OW), which is defined by

$$OW = \psi_{xy}^2 - \psi_{xx}\psi_{yy} \tag{2.3}$$

where ψ is the streamfunction. Eq. (2.3) is precisely the magnitude of the rate of strain squared minus the rate of the rotation squared, that is, the radical in (2.1).

As an example we have plotted the OW parameter in Figure 2.1 on top of SSH anomalies. In this case our detection scheme has registered four points where a negative OW value overlaps with a SSH extremity and a geostropic velocity minima. We also see a lot of areas where the OW parameter alone would have given us a false eddy (the other blue spots). This is avoided because we demand that they have a corrsponding maxima or minima in the SSH anomaly.

We find that the detection scheme is highly dependant on the smoothing of the SSH field. After finetuning we concluded that smoothing by averaging over 49 points was optimal. This removed edges and got rid of noise in the SSH anomaly field while retaining the structures recogniseable as highs and lows. Following *Isern-Fontanet et al.* (2006) we put the Okubo-Weiss treshold to be zero as this gives better accuracies for areas with small OW variance. We have discarded any eddies with a radius larger than a hundred kilometer as they would be unrealistic for our domain. This is to circumvent a known problem with the detection method where it may register ocean gyres as eddies.

Due to the fine resolution of our SSH anomaly field we have opted to differentiate height contours with a 0.8 cm height difference rather than the 2.0 cm usually employed in the detection scheme. This is because the NorKyst800 grid is finer than satellite altimetry data, which was the assumption by in the Penven scheme. A Hanning filter was applied to the the OW parameter to remove noise. We found that there was no benefit to applying it more than once and so it was only done once for computational efficiency.

2.3 Kinetic energy diagnostics

In addition to an eddy detection method, we also make a kinetic energy diagnostic along the lines of *Røed and Fossum* (2004) and *Albretsen and Røed* (2010). The rationale is to possibly correlate areas where eddies are numerous with areas of high eddy kinetic energy.

For all calculations we use the depth averaged velocity fields from NorKyst800. According to *Røed and Fossum* (2004) and *Albretsen and Røed* (2010) a time average of a little less than a month should be a sufficient time period to average out the eddies from the mean flow. Because of the limit in size of our available dataset, and because we want to be able to look at seasonal variations, we choose 60 days as our averaging period. The choice of time averaging is discussed

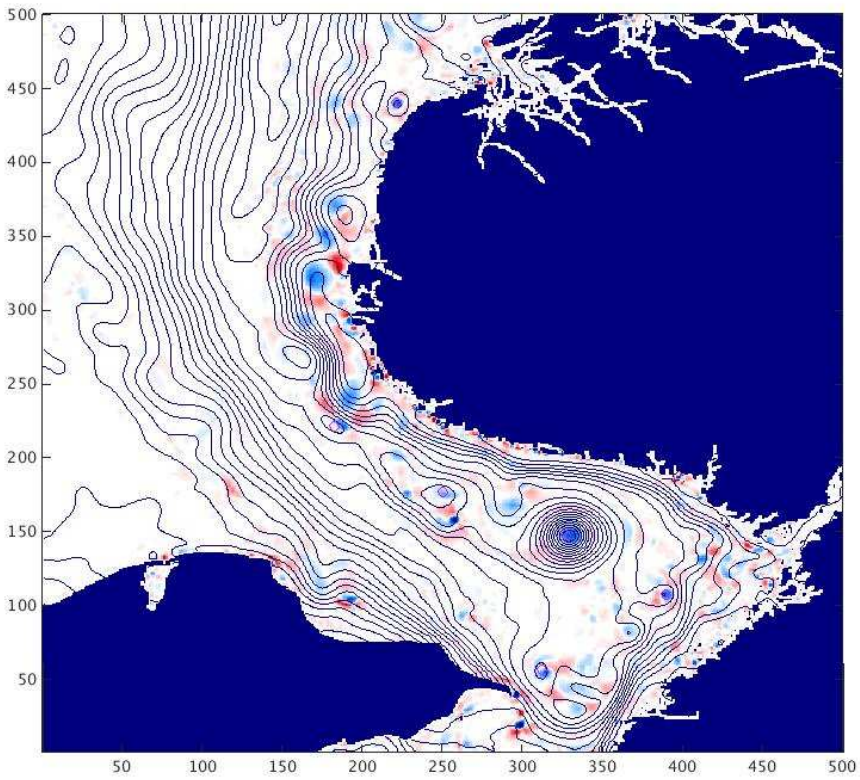

Figure 2.1: Displayed is the Okubo-Weiss parameter (OW) from a random day in the period 2013-2014. Blue colors denote areas of where vorticity dominates over strain ($OW < 0$), while red colors denote area where strain dominates $OW > 0$. Solid black curves denote smoothed isolines of sea surface height. Small red circles indicate points where the detection scheme has discovered eddies (a total of four).

in some more detail in Section 4.1 below. From NorKyst800 we extract the two components U and V of the depth avaraged velocity to form the velocity $\mathbf{u}$. The time average or the mean motion is then defined by

$$\bar{\mathbf{u}} = \frac{1}{2T} \int_{t-T}^{t+T} \mathbf{u}(x, y, t)\, \mathrm{d}t. \tag{2.4}$$

where $T = 30$ days. This gives a total of 12 such averages in our dataset. It should be noted that beause of gaps in the series of available NorKyst800 model results, the last average contains less than 60 days. This is why this period is excluded in some of the results. As we have seen, this should be sufficient to avoid most of the influence of the eddies on the mean current.

The deviation from the mean velocity $\bar{\mathbf{u}}$ and the daily velocity $\mathbf{u}$ is denoted $\mathbf{u}'$, and is given by

$$\mathbf{u}' = \mathbf{u} - \bar{\mathbf{u}} \tag{2.5}$$

We note that $\overline{\mathbf{u}'} = 0$. It then follows,

$$\overline{\mathbf{u}^2} = \overline{(\bar{\mathbf{u}} + \mathbf{u}')} \cdot \overline{(\bar{\mathbf{u}} + \mathbf{u}')} = \overline{\bar{\mathbf{u}} \cdot \bar{\mathbf{u}}} + 2\overline{(\bar{\mathbf{u}} \cdot \mathbf{u}')} + \overline{\mathbf{u}' \cdot \mathbf{u}'}. \tag{2.6}$$

Since

$$\overline{(\bar{\mathbf{u}} \cdot \mathbf{u}')} = \bar{\mathbf{u}} \cdot \overline{\mathbf{u}'} = 0 \tag{2.7}$$

we get

$$\overline{\mathbf{u}^2} = \bar{\mathbf{u}}^2 + \overline{\mathbf{u}'^2}. \tag{2.8}$$

The average kinetic energy per unit mass, henceforth KE, is defined by

$$KE = \frac{1}{2}\overline{\mathbf{u}^2} = MKE + EKE, \tag{2.9}$$

where

$$MKE = \frac{1}{2}\bar{\mathbf{u}}^2 \quad \text{and} \quad EKE = \frac{1}{2}\overline{\mathbf{u}'^2}. \tag{2.10}$$

Thus MKE is the mean kinetic energy, or the kinetic energy associated with the mean motion. EKE, or "Eddy kinetic energy" is then the kinetic energy contributed due to the variance $\mathbf{u}'^2$. In practice KE and MKE is computed as above while EKE is simply evaluated by subtracting MKE from KE, or

$$EKE = KE - MKE. \tag{2.11}$$

The variance $\mathbf{u}'^2$ is amongst other things used by our algorithm below to find the stationary points in the detection scheme.

We use these kinetic energy values for the energy comparisons performed in Chapters 3 and 4 three and four.

Chapter 3

Results

3.1 Size distribution of eddies

As we see from Figure 3.1 anticyclones are in general somewhat bigger than cyclones and they rarely have radii below 5 km, wheras a substantional amount of the cyclones have radii below this level. We see that the distribution for anticyclones peak between six and seven kilometres in radius while the corresponding peak for cyclones lies between five and six kilometres. From Figure 3.2 we also see that the anticyclone distribution has a longer and more pronounced tail which means that the anticyclones overall are larger than cyclones.

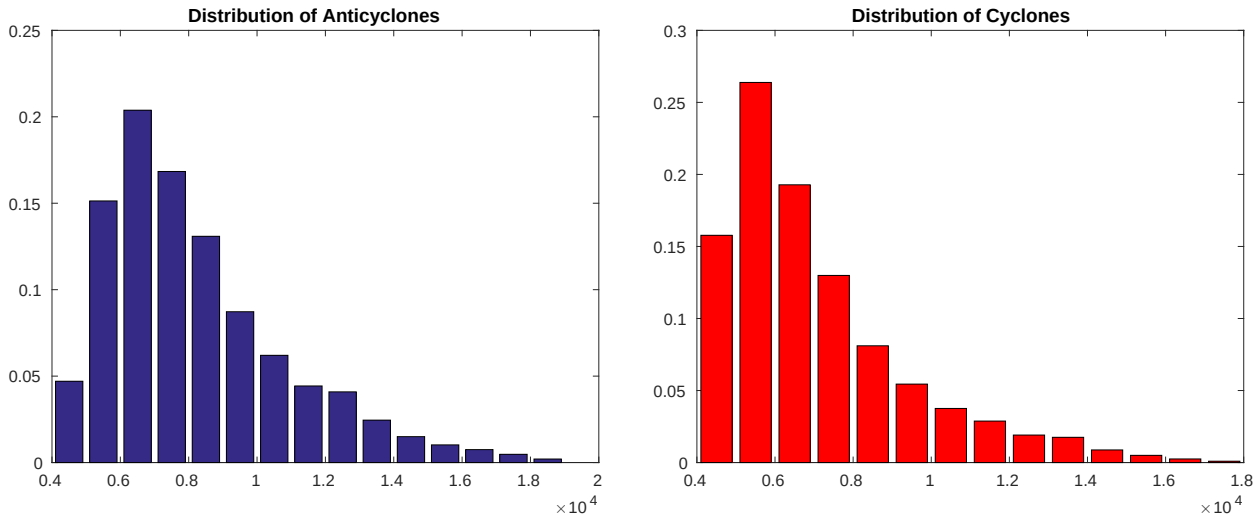

Figure 3.1: The size distribution of anticyclones (left) and cyclones (right) in the Skagerrak. Eddies of radii smaller than 4 km are cut off to reduce noise. Both anticyclones and cyclones are normalized to illustrate their distribution. These graphs does not show if cyclones or anticyclones is the most prevalent within our domain. The horizontal axis gives the radius in metres, while the y-axis shows fraction.

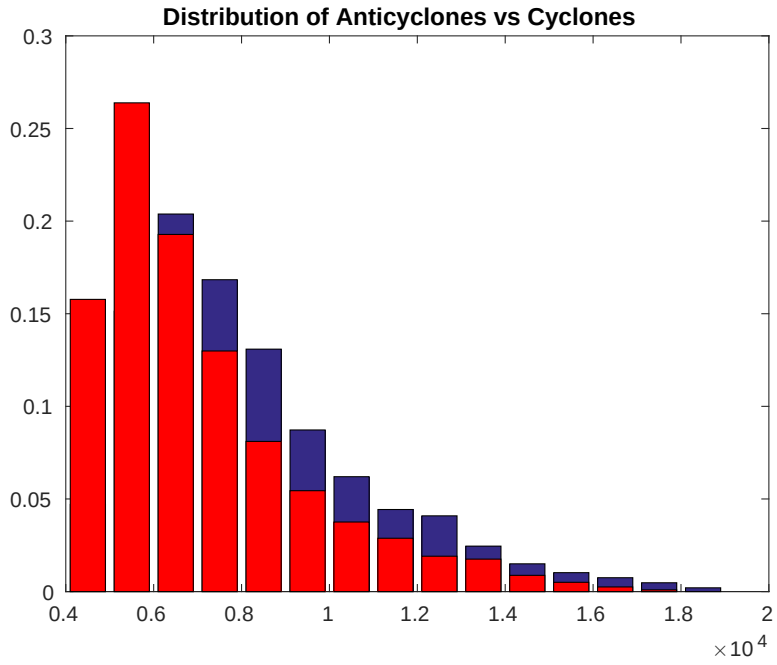

Figure 3.2: This graph is the two graphs from Figure 3.1 on top of each other for easier reference. The blue bars represent anticyclones and the red cyclones.

3.2 Eddy Census

To reduce noise while retaining information we have cut the eddy radius at 4 km for the cyclones and at 7 km for the anticyclones in Figure 3.3. From the distributions in Figure 3.1 we see that this is before the respective peaks of the two signals and thus we feel confident that little information is lost. Furthermore we have binned occurrences into 2x2 km boxes and have counted the number of times an eddy has occurred in each square over the two year period 2013-2014. The first thing we see from Figure 3.3 is that the occurrences of anticyclones are much more rare and occurrences of cyclones are more prevalent. Some of the bright spots we see in Figure 3.3 are actually larger than the maximum scale (30 occurrences). In contrast the highest number of occurences for the anticyclones are less 25.

Also apparant in Figure 3.3 is that there are hardly any eddies registered in the jet currents. As we see from the cyclone frequency plot of Figure 3.3, there appears to be two hotspots where cyclones are more frequent. Both are within the Norwegian Trench. One of these lies in the middle of the deepest part of the Trench, while the other one is outside off Arendal. As we see in Fig 3.4, where we have reduced the maximum number of occurrences shown down to 15 occurrences, there is a rather visible field in the deeper part of the trench where cyclones pops up quite frequently.

For the anticyclones we see that there are a few spots where they are more likely to be found. This is in contrast to what we found for the cyclones. To the east of Skagen (the northern tip

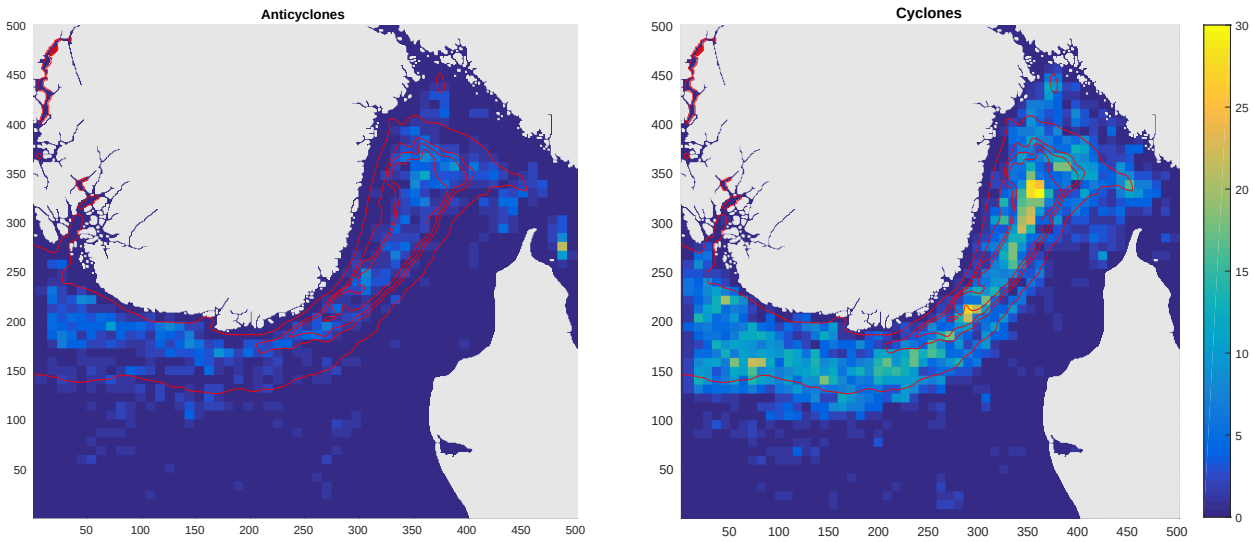

Figure 3.3: Displayed is the frequency of occurrence of anticyclones (left) and cyclones (right) in the Skagerrak. The color bar indicates the frequency of occurrence in the range 0 to 30. The red lines indicate bottom depth at 200, 400, 450 and 500 m, respectivly. Numbers along axes denote grid number in the NorKyst800 model.

of Denmark) there is a particularly spot of high occurrences of anticyclones. We also see quite a few anticyclones being formed in the inner and deepest part of the Norwegian Trench, we see some being formed outside of Torungen/Arendal where there is a bulge in the Trench, which sometimes correlates with a bulge in EKE. And finally we see anticyclones appearing south and west of Lista in line with (*Fossum and Røed*, 2006). While there seems to be the same spot in the Trench that anticyclones and cyclones appears, closer scrutiny reveals this not to be the case, the anticyclone hotspot is slightly to the northeast of the centres of the cyclones.

3.2.1 Time dependence

To study the seasonal variation, as shown in Figures 3.5 - 3.8, we have binned occurrences into 2x2 km boxes and have counted the number of times an eddy has occurred in each square over the respective periods (mostly 60 days). As we see from Figure 3.5 and 3.6 both the intensity of cyclones and anticyclones varies a lot with the seasons with the summer months showing very few eddies of either kind appearing. But in spring and autumn we see a difference between anticyclones and cyclones as there seems to be less variance in the amount of cyclones between autumn winter and spring than for anticyclones. The period of the February 25, 2014 to April 28, 2014 was a bit of an anomaly, but we choose to include it in the seasonal variance plots. It varied from the norm of the typical spring with the “Dot” of eddies in the inner part of the trench, as it is worth noting and will be discussed.

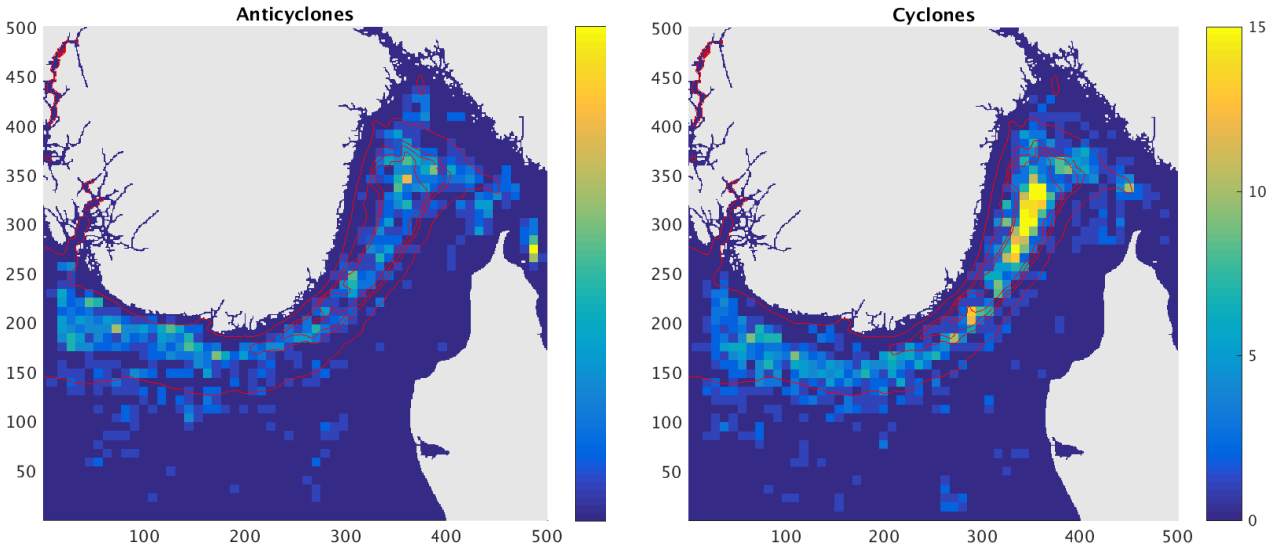

Figure 3.4: The figures show the frequency of cyclones and anticyclones occurrences. To the left are the occurrences of anticyclones and to the right cyclones. Both cyclones and anticyclones are cut at 7 km radius minimum. This removes a lot of the smaller Cyclones. The red lines are bottom topography curves for 200, 400, 450 and 500 metres, respectively.

3.3 An energy analysis

Below, we give an overview of the kinetic energy and the direction of the mean currents from Section 2.3 to give a better picture of the currents and jets involved, and their strenghts and how this changes throughout our time period.

As we see from Figures 3.9 - 3.11 the 60 day average kinetic energy of the currents changes a lot throughout the year. They seem to be the most energetic during the winter months, and least during the summer months. We also see that there is a tendency for there to be a lot of kinetic energy in the shallower areas west of Denmark. The intensity and width of the NCC also seems to vary with the seasons. It becomes more narrow and energetic during the spring and autumn months. This fits well with what we see from the EKE plots depicted by Figures 3.12 and 3.13. Together the KE and EKE plots give a good identication of how much total kinetic energy the system has available at various times, and how much of it is due to the variance.

Like with the total average kinetic energy we see a lot of seasonal variability in the EKE or the variance. Looking at Figure 3.12 and contrasting June-Aug 2013 with August to october 2013 and Dec 2013 to feb 2014 for example, we clearly see how the EKE builds up towards a peak at the winter from the really unenergetic summer conditions and how the energy then ebbs towards the summer.

Of particular note, In the EKE plot for February to March 2013, In Figure 3.13 we see a clear bulging in the NCC outside of Torungen which is a clear sign of cyclogenisis. We also

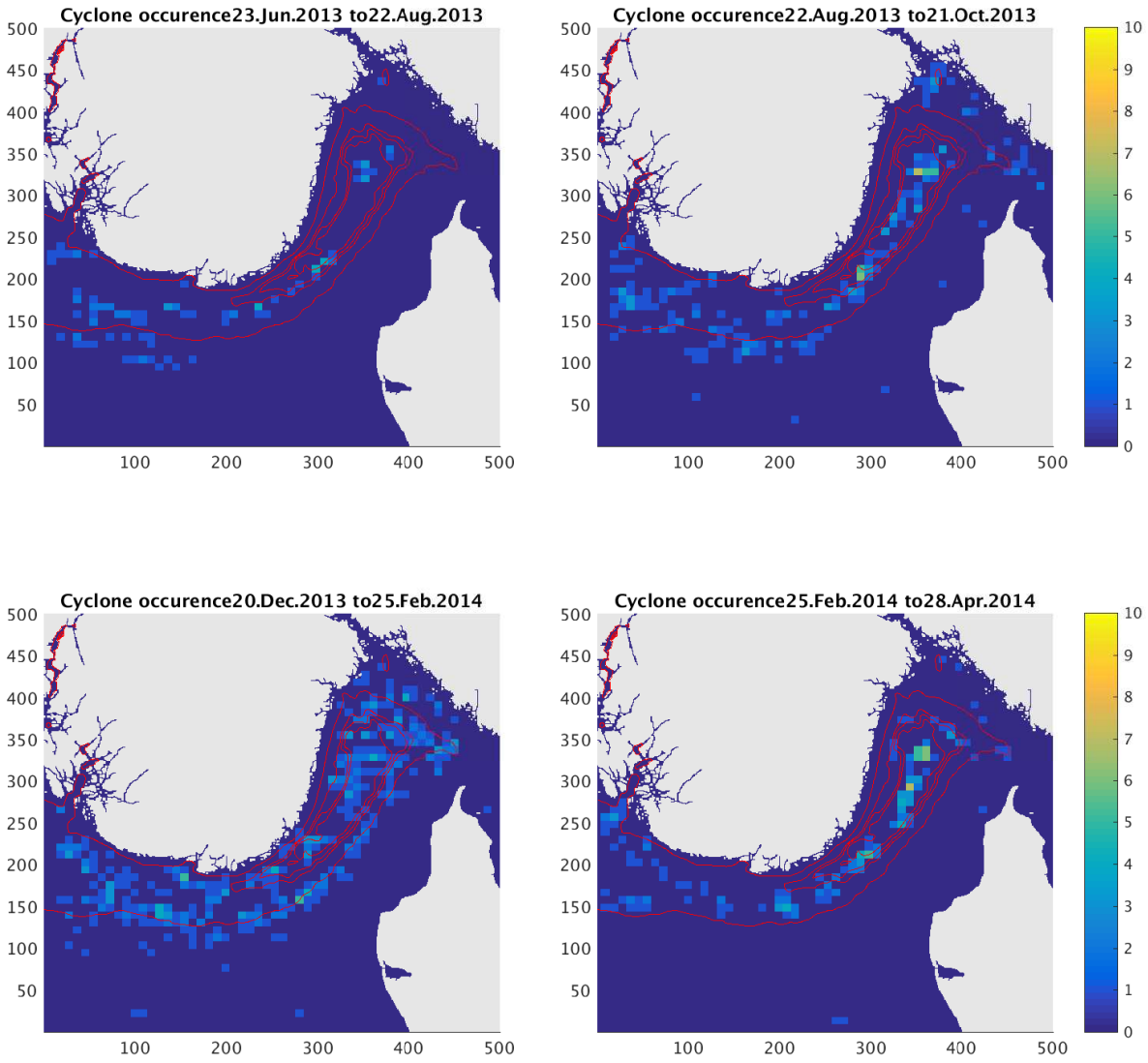

Figure 3.5: Shown are the frequency of cyclones in the Skagerrak for four periods representative of their seasons. The color bar indicates the frequency of occurrence in the range 0 to 30 day^{-1}. The red lines indicate bottom depth at 200, 400, 450 and 500 m, respectivly. Numbers along axes denote grid number in the NorKyst800 model.

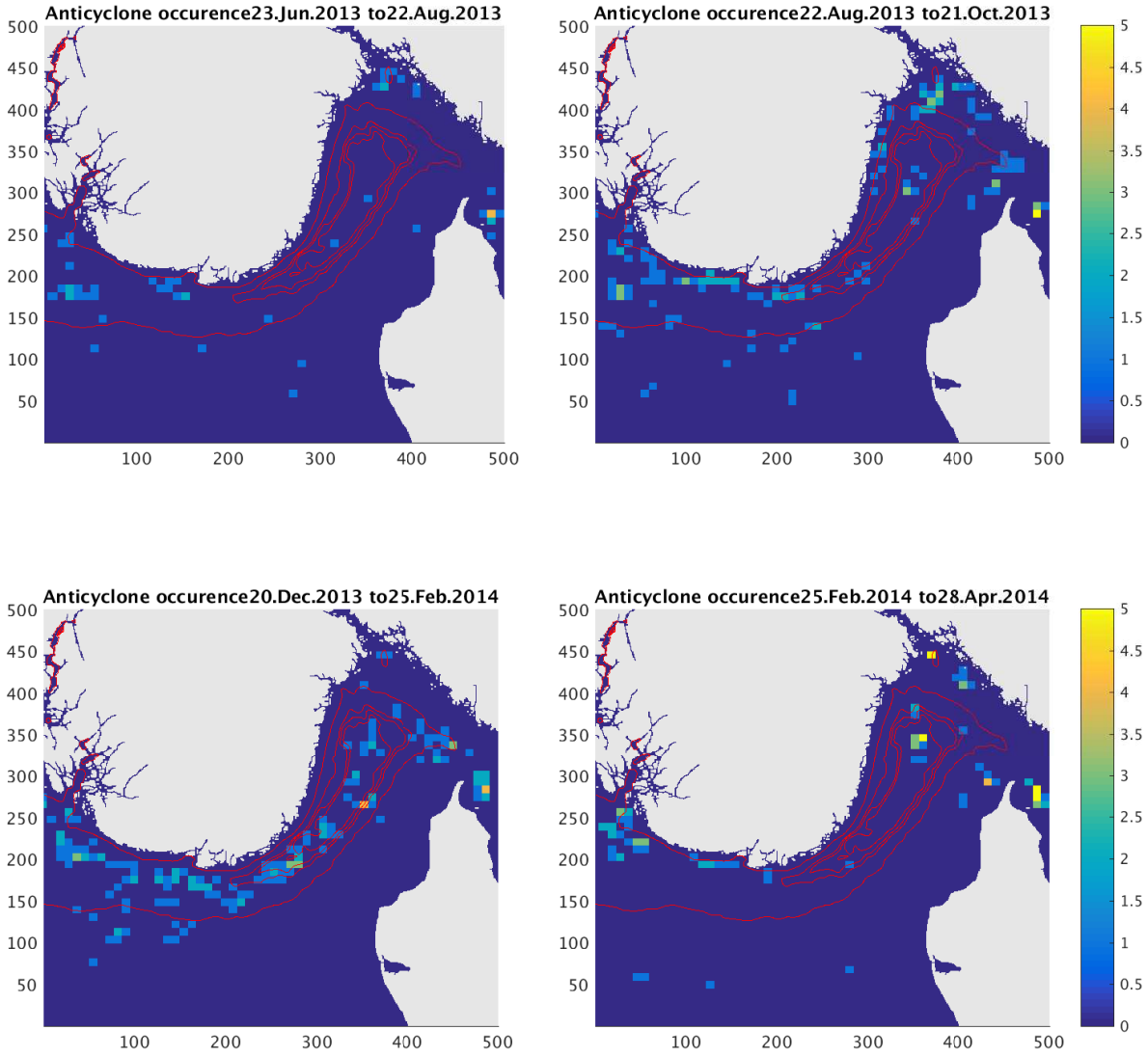

Figure 3.6: Shown are the frequency of anticyclones in the Skagerrak for four periods representative of their seasons. The color bar indicates the frequency of occurrence in the range 0 to 30. The red lines indicate bottom depth at 200, 400, 450 and 500 m, respectivly. Numbers along axes denote grid number in the NorKyst800 model.

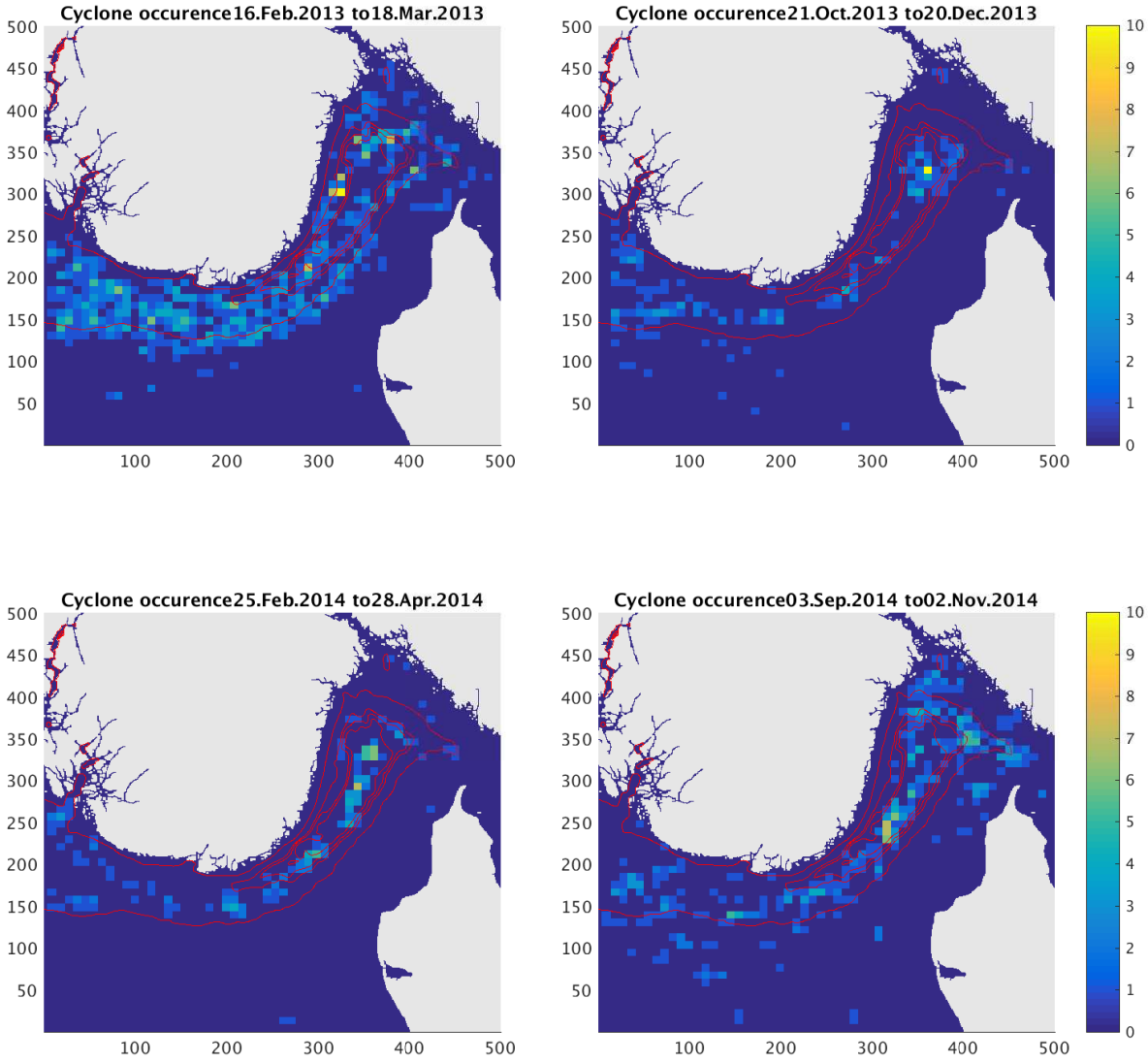

Figure 3.7: Displayed is the frequency of occurrence of cyclones for periods we found particularly energetic in the Skagerrak. The color bar indicates the frequency of occurence in the range 0 to 30 day^{-1}. The red lines indicate bottom depth at 200, 400, 450 and 500 m, respectivly. Numbers along axes denote grid number in the NorKyst800 model This graph shows other seasons with detected Anticyclones of note.

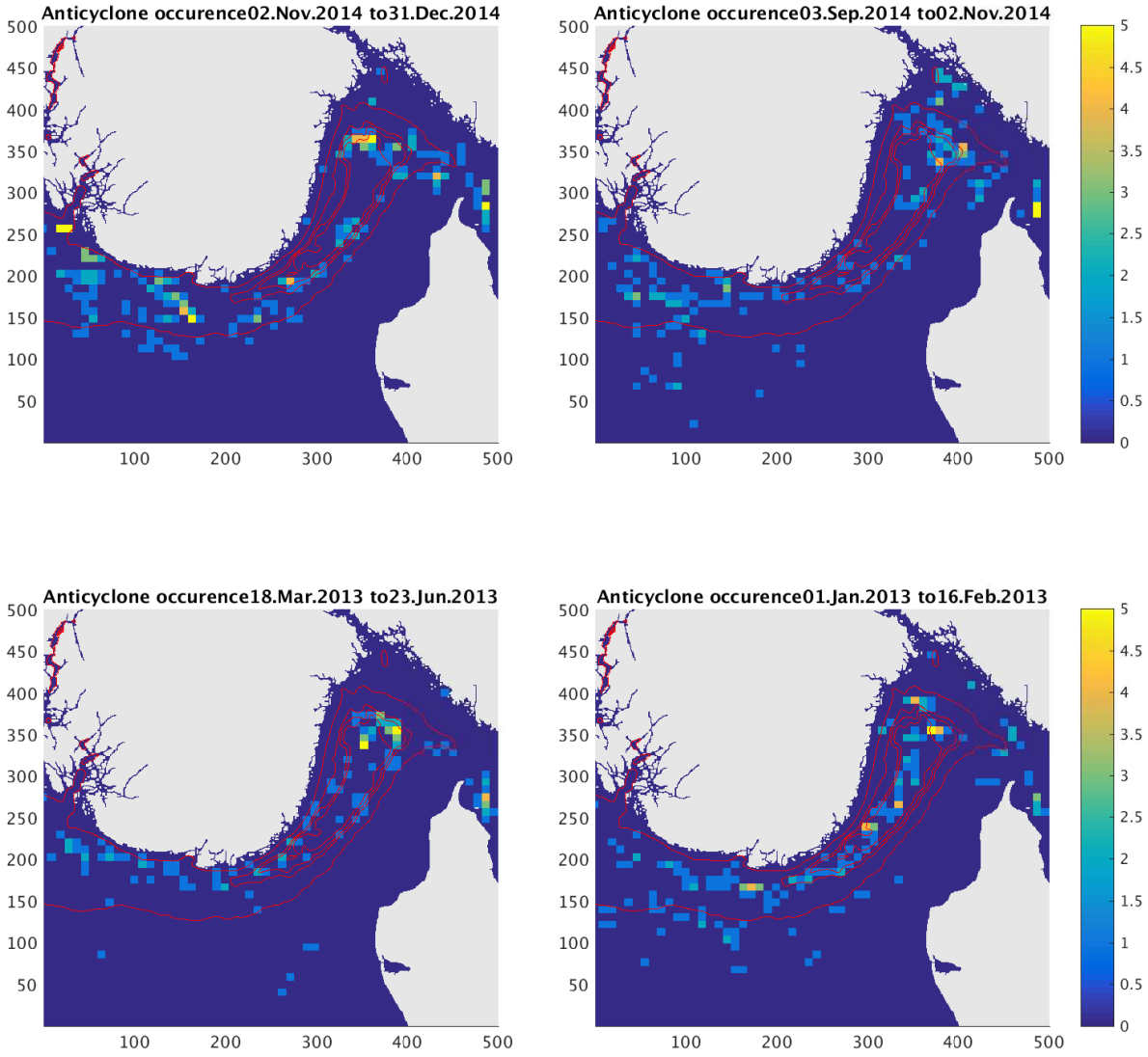

Figure 3.8: Displayed is the frequency of occurrence of anticyclones for periods we found particularly energetic in the Skagerrak. The color bar indicates the frequency of occurrence in the range 0 to 30. The red lines indicate bottom depth at 200, 400, 450 and 500 m, respectivly. Numbers along axes denote grid number in the NorKyst800 model This graph shows other seasons with detected Anticyclones of note.

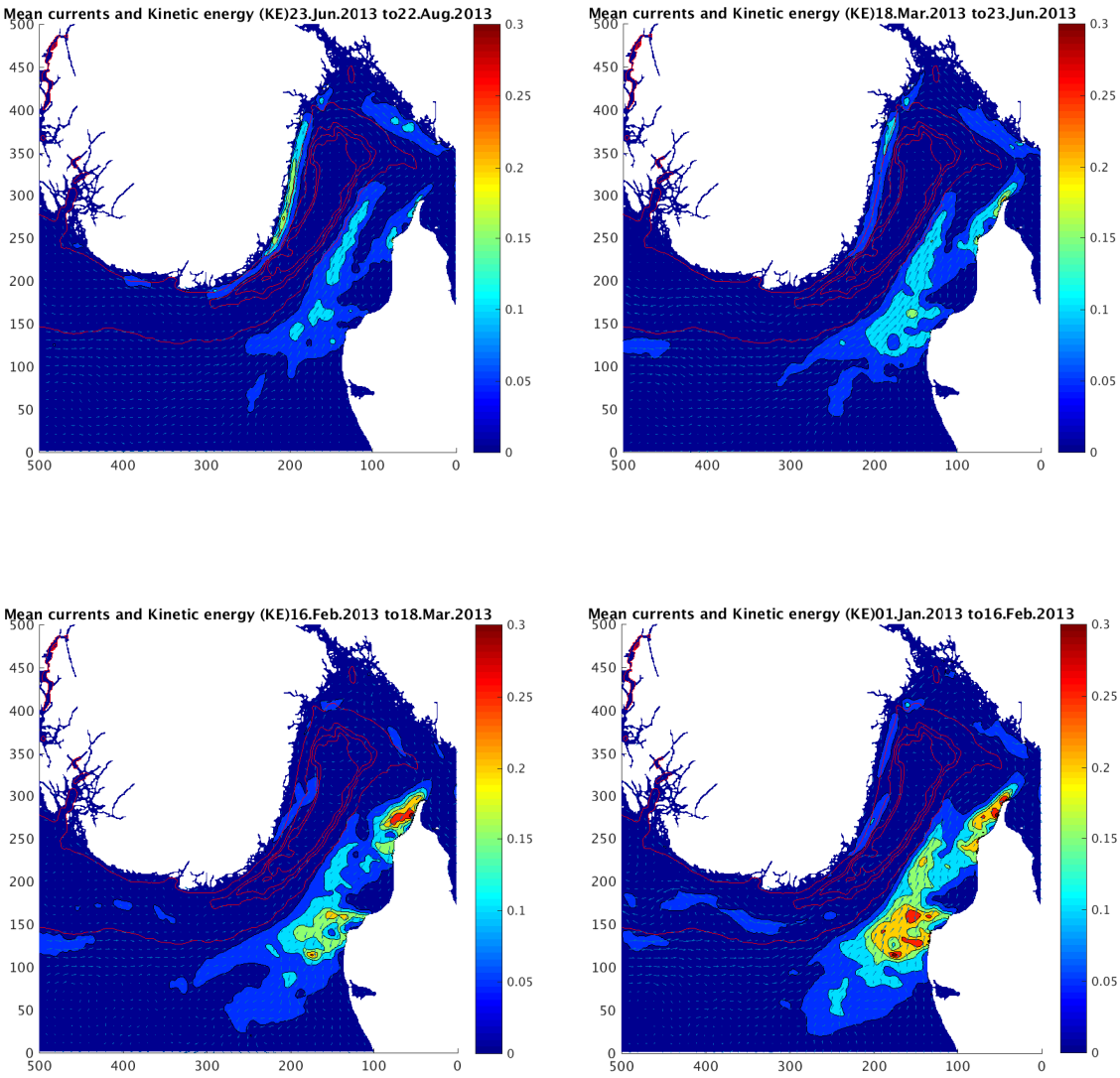

Figure 3.9: This graph shows the mean currents and the average kinetic energy (KE) for the first four 60 day averaging periods (exept lower right which is 40 days). The colorbar is given in $\frac{m^2}{s^2}$. The results were not divided by two. so it shows $2KE$.

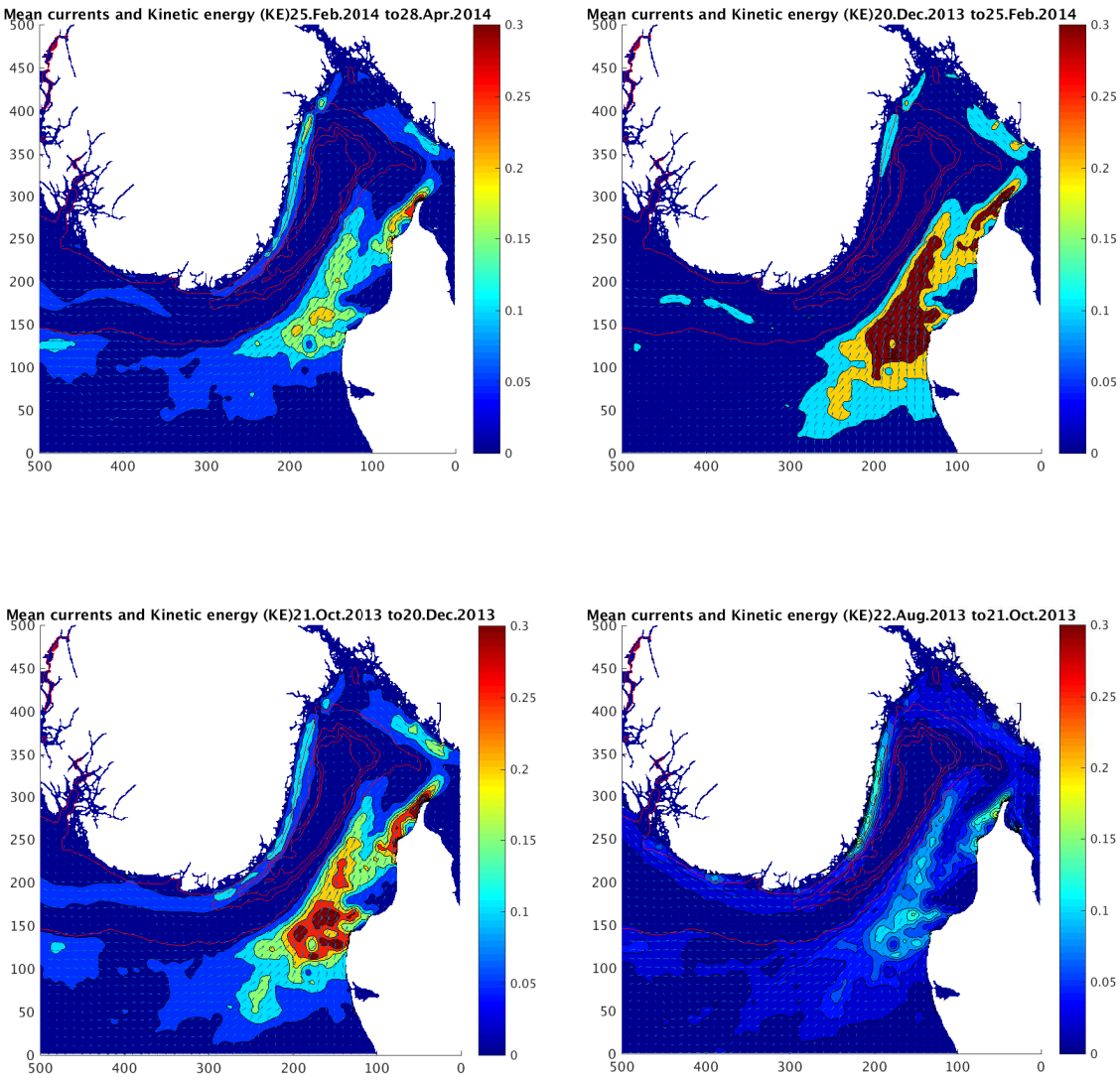

Figure 3.10: This graph shows the mean currents and average kinetic energy for the fifth to eight 60 day averages of our dataset. The colorbar is given in $\frac{m^2}{s^2}$. The results were not divided by two, so it shows $2KE$.

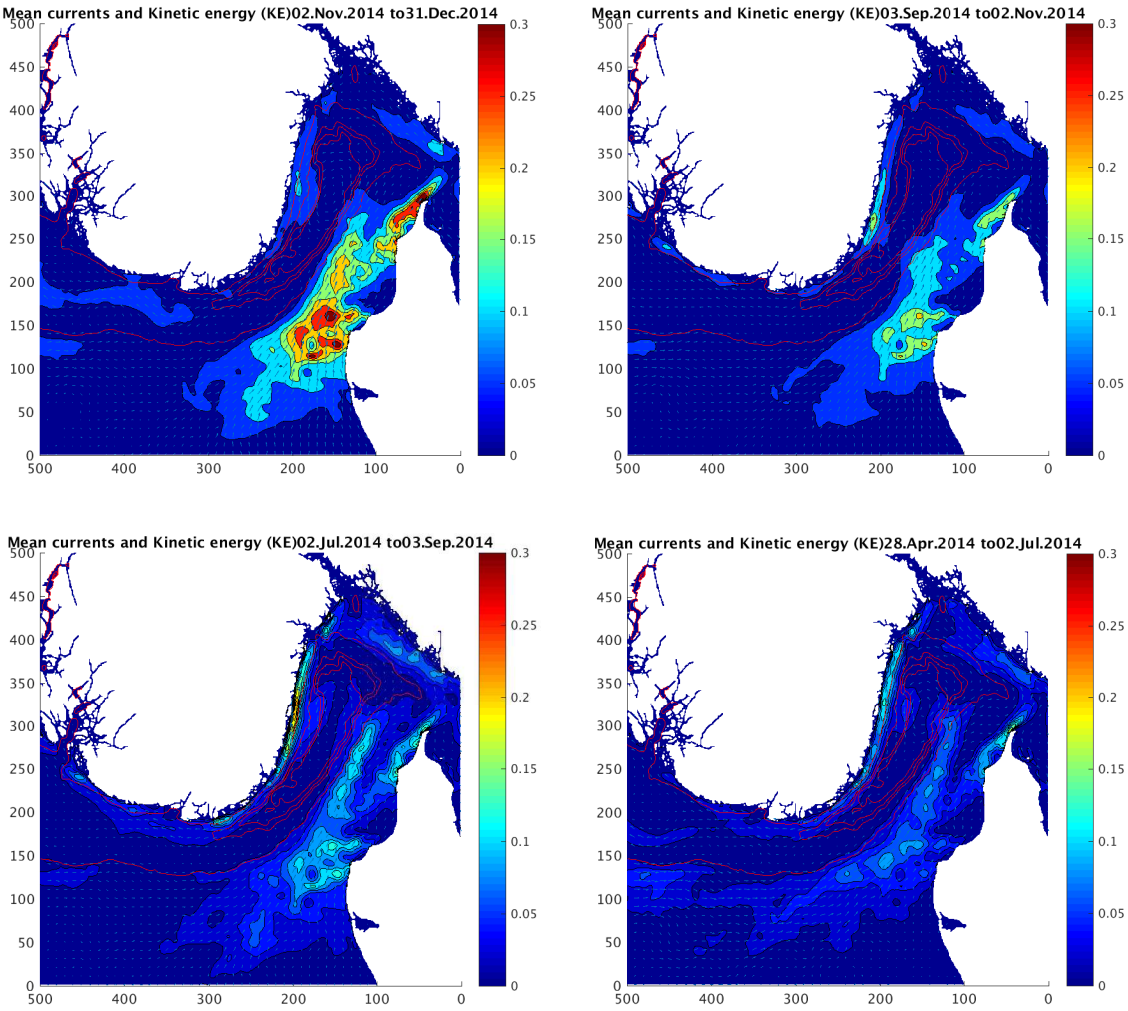

Figure 3.11: This graph shows the mean currents and average kinetic energy for the last four 60 day averages of our dataset. The colorbar is given in $\frac{m^2}{s^2}$. The results were not divided by two, so it shows $2KE$.

see this for September 3, 2014 - November 2, 2014, but in a weaker form. Thus it is clear that this is an area where we expect to see cyclogenesis and instabilities to appear. Also of note in Figure 3.13 is a weak circular shape around the inner part of the Norwegian Trench in the period February to April 2014. The strength is between 0.1 and 0.2 $\frac{m^2}{s^2}$, which indicates that the currents in this area during this period have been dominated by a circular motion or eddies. This is explored a bit more in detail in the discussion section below.

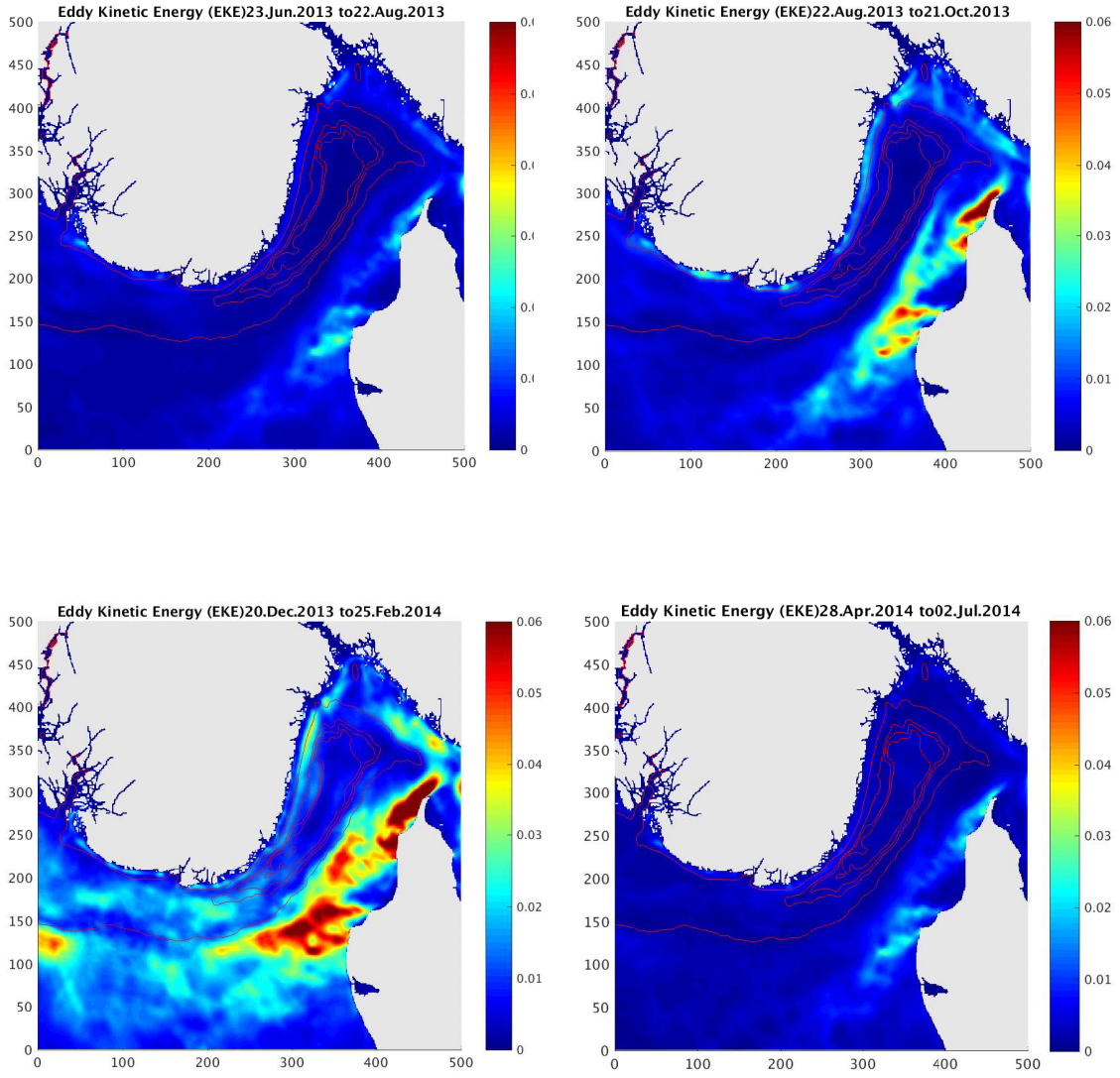

Figure 3.12: The graph shows four averages of EKE representative of their respective seasons according. The colorbar is given in $\frac{m^2}{s^2}$.

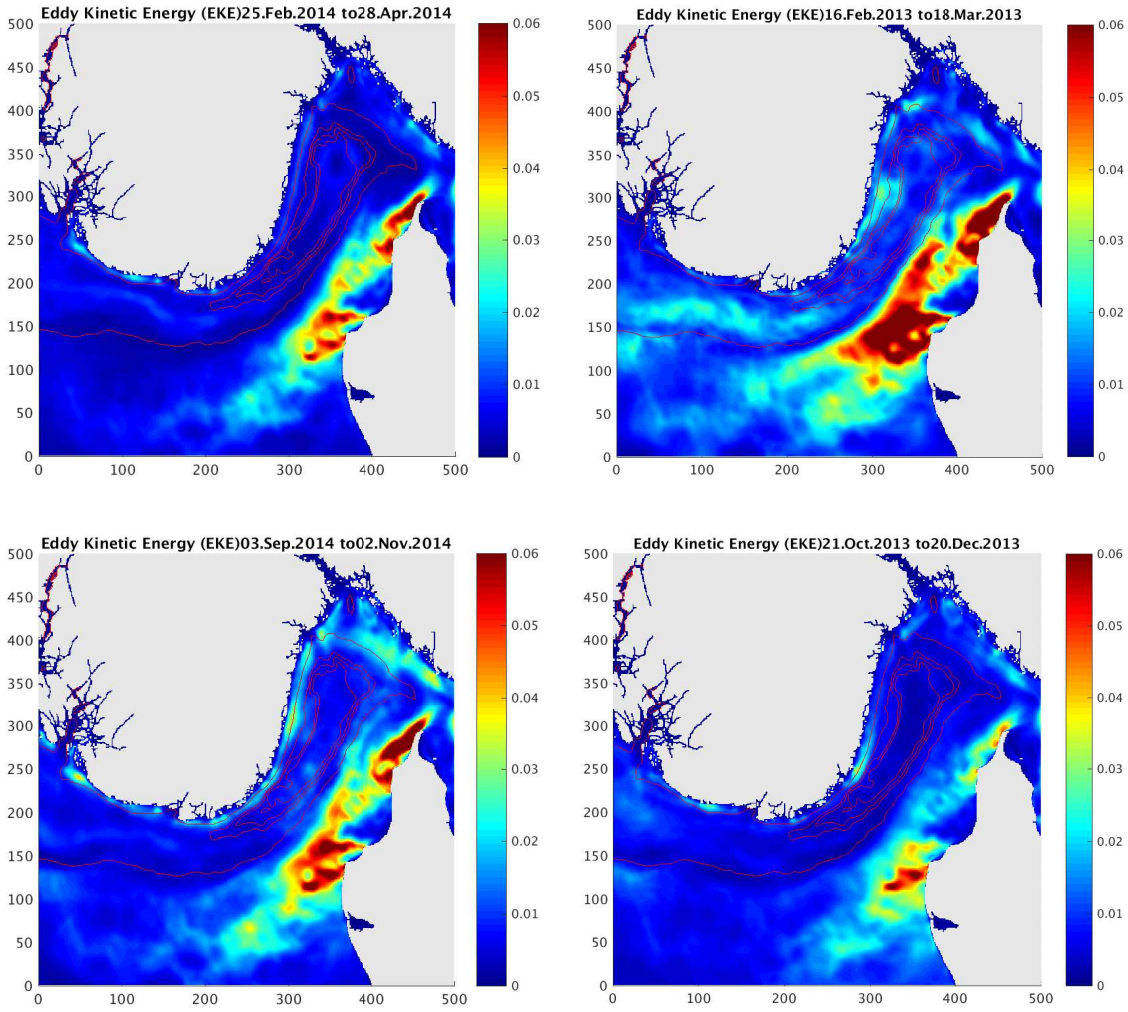

Figure 3.13: . This graph shows the EKEs for four averaging periods (see top of each panel for period covered). The colorbar is given in units of $\frac{m^2}{s^2}$.

Chapter 4

Discussion

4.1 The choice of time averaging

In the method chapter we choose to use a sixty day average of the current to create current averages and from them extract EKE. The question that arise is whether this is a long enough period to average out the effects of eddies?

Røed and Fossum (2004) performed a spectral analysis of the currents and found that the time scales that corresponded to the mesoscale eddies in the Lista area had a time frame of two to ten days. They thus concluded that the ideal would be to average over two weeks or more. *Petersen et al.* (2013) found that less than 25 percent of the eddies last for a full month. They also found a clear positive correlation between eddy diameter and lifetime. In the area in question the baroclinic Rossby radius is about 10-16 km, much smaller than the typical oceanic eddies. Thus we would expect our much smaller eddies to last even shorter. Averaging over a full month should therefore cancel out most of their effect.

However, as found by *Schlax and Chelton* (2008), no matter how long a period you average over it is impossible to completely remove the effects of eddies on the background field because of their anisotropy. This will bias the regionally averaged velocity fields and thus bias our eddy detection scheme. Therefore it does not seem possible to completely remove this bias. For example in the "odd" period between the February 25, 2014 to April 28, 2014 we saw that there existed a mean current with a substantial total kinetic energy around the eddies, likely generated by the eddies. This entails that the EKE for this area and period was underestimated. In this case averaging over a longer timescale may have mitigated this.

In other words, the fact that eddies do not appear completely at random and have anisotropic traits means that they will have an impact on the mean field. Since we look for variations from the mean field to spot eddies and define EKE, this may cause an underestimation of the EKE, end hence in the number of eddy occurrences in areas where eddies are frequent.

Alongside the wish for reducing the impacts of eddies on the background field, we also wanted information about temporal variance, that is how eddies locations and numbers changed with season. In summary, the longer time one averages over, the more of the eddies impact on the background field is removed and the eddies easier to pick out. However, the longer the averages,

the less we can say about how our system changes with time. Thus we ended up with a sixty day averaging as a compromise.

4.2 Correlation between energy and eddies

As we saw in the results above, comparing Figure 3.5 and 3.6 with Figure 3.12, there is a rather clear visual correlation between areas of enhanced eddy kinetic energy and the amount of eddies we see appearing around the NCC and in the Norwegian Trench in their respective seasons. Yet this strong correlation does not hold for the entire study area. As we saw in Figure 3.3 there were hardly any eddies appearing in the Jutland current, yet we saw in Figures 3.12 and 3.13 that there was a lot of variance or EKEin the Jutland current. This may be a symptom of the high impact of winds on the currents. As the currents pass over the very shallow depths along the coast of Denmark the effect of wind can easily reach the full depth and dominate the average current, and so the current has a lot of variance in its strenght without having any eddying motion. Indeed in some of our 60 day current means we see a lot of changes in strenght along the current. In a few cases we even saw a reversal of the current where water was being transported out of Kattegat towards the German Bight rather than towards the Swedish coast.

We also saw in the results, particularly depicted by Figures 3.4 and 3.8 (bottom right panel), that between January 1, 2013 and February 16, 2013 a lot of anticyclones appeared outside of Torungen/Arendal. This happens in an area where we see a bulge in the Trench which correlates in some cases with bulges in the energy plots as exemplified by Figure 3.13 (the two rightmost panels).

As we saw from Figures 3.5 and 3.6 the "odd" period between the February 25, 2014 to April 28, 2014 showed an abnormal amount of both cyclones and anticyclones appearing in the inner and deepest part Norwegian Trench for this season. This is when we had a somewhat enhanced ring of eddy kinetic energy around this area (cf. Figure 3.13). This fits more with traditional theory where cyclones and anticyclones are created in pairs. This may suggest that a different mechanism may be at work here than what we see during the other periods.

Chapter 5

Summary and conclusion

It is well known that cyclonic and anticyclonic eddies are numerous in the Skagerrak. Nevertheless a systematic analysis of their statistics appears to be missing. This is attempted in the present thesis applying an eddy detection method as outlined in Section 2.2. In addition we perform a kinetic energy analysis discriminating between the mean kinetic energy and the the eddy kinetic energy (Section 2.3). The "data" we use are the 24 hour average daily snapshots produced by MET Norway's operational coastal ocean forecasting model NorKyst800. The period we study is the two years 2013 and 2014 which results in about 700 snapshots.

We find that overall there are more cyclones than anticyclones (Figure 3.3 and 3.4), that there is a strong correlation between kinetic energy and generation of eddies (Figure 3.5, 3.6 and Figure 3.12), that in genera most of the eddies prefer to be within the Norwegian Trench area (Figure 3.4), and that the eddies are more frequent in three specific areas along the Trench, namely the inner and deepest part of the Trench, outside of Torungen/Arendal and south Lista at the the southern tip of Norway (Figure 3.3). It is also interesting to note that despite the very high values of variance and EKE shown in the currents outside of Denmark, almost no eddies appear in them.

In addition we find that there is substantial seasonal variations in both in eddy occurence and total and eddy kinetic energy as found in Section 3.2.1. We see here that the Skagerrak basin is more energetic in winter and less so in summer as shown by Figures 3.9 trough 3.13. This corresponds to more eddies appearing during winter than in summer (Figures 3.5 and 3.6).

We have also corroborated some of the findings of *Albretsen and Røed* (2010). We find high occurrences of eddies in the Norwegian Trench, while they found enhanced eddy kinetic energy there, and assumed that it was caused by eddy ocurences. This clearly demonstrates the need for a high resolution models to resolve the mesoscale processes in the Skagerrak.

For future studies it would be interesting to look deeper into mechanisms for instability and do a full analytical stability analysis, looking into amongst other things whether the Kelvin-Helmholtz model is applicable to our domain.

Bibliography

Albretsen, J. (2007), The impact of freshwater discharges on the ocean circulation in the Skagerrak/northern North Sea area. Part II: Energy analysis, *Ocean Dynamics*, *57*, 287–304, doi:10.1007/s10236-007-0121-6.

Albretsen, J., and L. P. Røed (2006), Sensitivity of Skagerrak dynamics to freshwater discharges: insight from a numerical model, in *European Operational Oceanography: Present and Future, Proceedings of the 4th International Conference o n EuroGOOS, 6-9 June 2005, Brest, France*, edited by H. Dahlin, N. C. Flemming, P. Marchand, and S. E. Petersson, pp. 773–779, EuroGOOS Office, SMHI, and European Commission Research Directorate.

Albretsen, J., and L. P. Røed (2010), Decadal long simulations of mesoscale structures in the North Sea/Skagerrak using two ocean models, *Ocean Dynamics*, *60*, 5–36, doi:10.1007/s10236-010-0296-0.

Albretsen, J., A. K. Sperrevik, A. Staalstrøm, A. D. Sandvik, F. Vikebø, and L. C. Asplin (2011), Norkyst-800 Report No. 1: User manual and technical descriptions, *Tech. Rep. Fisken og Havet 2/2011*, Institute of Marine Research, Pb. 1870 Nordnes, N-5817 Bergen, Norway.

Basdevant, C., and T. Philipovitch (1994), On the validity of the "weiss criterio" in two-dimensional turbulence, *Physica D: Nonlinear Phenomena*, *73*(1-2), 17–30.

Blumberg, A., and G. Mellor (1987), A description of a three-dimensional coastal ocean circulation model., in *Three-dimensional Coastal Ocean Models*, *Coastal and Estuarine Sciences*, vol. 4, edited by N. Heaps., pp. 1–16, American Geophys. Union.

Chelton, D. B., M. G. Schlax, R. M. Samelson, and R. A. de Szoeke (2007), Global observations of large oceanic eddies, *Geophysical Research Letters*, *34*(15).

Cushman-Roisin, B. (2016), Environmental fluid mechanics, to be published.

Fossum, I. (2006), Analysis of instabilities and mesoscale motion off southern Norway, *J. Geophys. Res.*, *111, C08006*, doi:10.1029/2005JC003228.

Fossum, I., and L. P. Røed (2006), Analysis of instabilities and mesoscale motion in continuously stratified ocean models, *J. Mar. Res.*, *64*, 319–353.

Haidvogel, D. B., H. Arango, P. W. Budgell, B. D. Cornuelle, E. Curchitser, E. D. Lorenzo, K. Fennel, W. R. Geyer, A. J. Hermann, L. Lanerolle, J. Levin, J. C. McWilliams, A. J. Miller, A. M. Moore, T. M. Powell, A. F. Shchepetkin, C. R. Sherwood, R. P. Signell, J. C. Warner, and J. Wilkin (2008), Ocean forecasting in terrain-following coordinates: Formulation and skill assessment of the Regional Ocean Modeling System, *J. Comput. Phys.*, *227*(7), 3595–3624, doi:http://dx.doi.org/10.1016/j.jcp.2007.06.016.

Isern-Fontanet, J., E. García-Ladona, and J. Font (2003), Identification of marine eddies from altimetric maps, *Journal of Atmospheric and Oceanic Technology*, *20*(5), 772–778.

Isern-Fontanet, J., E. García-Ladona, and J. Font (2006), Vortices of the mediterranean sea: An altimetric perspective, *Journal of physical oceanography*, *36*(1), 87–103.

Johannessen, J., E. Svendsen, S. Sandven, O. M. Johannessen, and K. Lygre (1989), Three-dimensional structure of mesoscale eddies in the Norwegian Coastal Current, *J. Phys. Oceanogr.*, *19*, 3–19.

Müller, M., M. Homleid, K.-I. Ivarsson, M. A. Køltzow, M. Lindskog, U. Andrae, T. Aspelien, D. Bjørge, P. Dahlgren, J. Kristiansen, R. Randriamampianina, M. Ridal, and O. Vignes (2015), AROME-MetCoOp: A Nordic convective scale operational weather prediction model, *Submitted*, -, –.

Okubo, A. (1970), Horizontal dispersion of floatable particles in the vicinity of velocity singularities such as convergences, *17*(3), 445–454.

Penven, P., V. Echevin, J. Pasapera, F. Colas, and J. Tam (2005), Average circulation, seasonal cycle, and mesoscale dynamics of the peru current system: A modeling approach, *J. Geophys. Res.: Oceans*, *110*(C10), doi:10.1029/2005JC002945, c10021.

Petersen, M. R., S. J. Williams, M. E. Maltrud, M. W. Hecht, and B. Hamann (2013), A three-dimensional eddy census of a high-resolution global ocean simulation, *J. Geophys. Res.: Oceans*, *118*(4), 1759–1774, doi:10.1002/jgrc.20155.

Røed, L. P. (1996), Modeling mesoscale features in the ocean, in *Waves and Nonlinear Processes in Hydrodynamics*, *Fluid Mechanics and its applications*, vol. 34, edited by J. Grue, B. Gjevik, and J. E. Weber, pp. 383–396, Kluwer Academic Publishers.

Røed, L. P., and J. Albretsen (2007), The impact of freshwater discharges on the ocean circulation in the Skagerrak/northern North Sea area. Part I: Model validation, *Ocean Dynamics*, *57*, 269–285, dOI: 10.1007/s10236-007-0122-5.

Røed, L. P., and I. Fossum (2004), Mean and eddy motion in the Skagerrak/northern North Sea: insight from a numerical model, *Ocean Dynamics*, *54*, 197–220.

Røed, L. P., N. M. Kristensen, and A. S. K. B. Hjelmervik (2016), A high-resolution, curvilinear roms model for the oslofjord. fjordos technical report no. 2, *met.no Report 4/2016*, Norwegian Meteorological Institute, Postboks 43 Blindern, N-0313 Oslo, Norway.

Sætre, R. (Ed.) (2007), *The Norwegian Coastal Current - Oceanography and Climate*, 159 pp., Tapir Academic Press, Trondheim, Norway, ISBN 978-82-519-2184-8.

Schlax, M. G., and D. B. Chelton (2008), The influence of mesoscale eddies on the detection of quasi-zonal jets in the ocean, *Geophys. Res. Lett.*, *35*, 56–72.

Shchepetkin, A. F., and J. C. McWilliams (2009), Correction and commentary for "Ocean forecasting in terrain-following coordinates: Formulation and skill assessment of the regional ocean modeling system" by Haidvogel et al., J. Comp. Phys. 227, pp. 3595-3624, *J. Comp. Phys.*, *228*(24), 8985 – 9000, doi:10.1016/j.jcp.2009.09.002.

Vallis, G. (2006), *Atmospheric and Oceanic Fluid Dynamics*, Cambridge University press.

Vallis, G. K., and M. E. Maltrud (1993), Generation of mean flows and jets on a beta plane and over topography, *J. Phys. Oceanogr.*, *23*, doi:10.1175/1520-0485(1993)023<1346:GOMFAJ>2.0.CO;2.

Weiss, J. (1991), The dynamics of enstrophy transfer in two-dimensional hydrodynamics, *Physica D: Nonlinear Phenomena*, *48*(2-3), 273–294.